Trends and rhythms in global seafloor generation rate

Jean-Pascal Cogné, Eric Humler

Geochemistry Geophysics Geosystems G3
AN ELECTRONIC JOURNAL OF THE EARTH SCIENCES
Published by AGU and the Geochemical Society

Article
Volume 7, Number 3
28 March 2006
Q03011, doi:10.1029/2005GC001148
ISSN: 1525-2027

Trends and rhythms in global seafloor generation rate

Jean-Pascal Cogné
Laboratoire de Paléomagnétisme, UMR CNRS 7577, Institut de Physique du Globe de Paris et Université de Paris 7, 4 Place Jussieu, F-75252 Paris Cedex 05, France (cogne@ipgp.jussieu.fr)

Eric Humler
Laboratoire des Géosciences Marines, UMR CNRS 7097, Institut de Physique du Globe de Paris et Université de Paris 7, 4 Place Jussieu, F-75252 Paris Cedex 05, France

Now at Laboratoire de Planétologie et Géodynamique, Université de Nantes, 4 Rue de la Houssinière, F-44322 Nantes Cedex 3, France (eric.humler@univ-nantes.fr)

[1] The primary purpose of this paper is to investigate the spreading and production rates of oceanic ridges for the last 180 Myr, based on the detailed analysis of eight oceanic units (North, Central, and South Atlantic basins, Southwest, Central, and Southeast Indian Ridge systems, Somalia basin, and the Pacific plate) and using the most recent timescale for oceanic isochrons. The global study of oceanic ridges presented here shows that (1) the average rate of spreading, which we computed by weighting the rates obtained at each basin by the relevant ridge lengths, is constant since ~125 Ma at 53.4 ± 5.9 mm yr^{-1} (full rate), (2) the average surface production rate is 2.7 ± 0.2 km^2 yr^{-1}, and (3) the minimum oceanic crust production in volume, or flux, is 18.7 ± 2.9 km^3 yr^{-1}. These estimations are in close agreement (within ±10%) with other studies. However, the new results emerging from this analysis are the following: (1) The Cretaceous flux rates (in volume) might be only 10% higher than today over a short period of time (125–100 Myr). (2) The "pulse" of ocean crustal production (120–80 Ma) in the world total is predominantly the result of contributions from mantle temperature and oceanic plateaus but is not linked to the global spreading rate of oceanic ridges, as generally accepted. (3) The rates presented here differ from previously published models for the Cenozoic and show a general increasing trend in the last 50 Myr. (4) We finally suggest a possible ~25 Myr pseudo-periodicity of the oceanic production rate (in surface and in volume) at least during the last 75–80 Myr. These data could have a profound impact on a vast number of models including sea-level changes and more generally on the chemical mass balance between ocean and continent, which is known to be a key parameter in the history of the Earth's climate and ocean chemistry.

Components: 9504 words, 5 figures, 4 tables.

Keywords: oceanic crust; production rates; spreading rates.

Index Terms: 1635 Global Change: Oceans (1616, 3305, 4215, 4513); 3035 Marine Geology and Geophysics: Midocean ridge processes; 4260 Oceanography: General: Ocean data assimilation and reanalysis (3225)

Received 22 September 2005; **Revised** 23 November 2005; **Accepted** 6 January 2006; **Published** 28 March 2006.

Cogné, J.-P., and E. Humler (2006), Trends and rhythms in global seafloor generation rate, *Geochem. Geophys. Geosyst.*, *7*, Q03011, doi:10.1029/2005GC001148.

1. Introduction

[2] It is generally thought that the ocean spreading rate at ridges has not been constant for the last 180 Myr; it may have attained two to four times its present-day value between 120 and 80 Ma (in the Cretaceous). Subsequent to this time, it has decreased [*Kominz*, 1984]. Because high spreading rates are believed to produce high topography of oceanic ridges [*Hays and Pitman*, 1973], this

variation of spreading rates in the past is considered to be a dominant forcing parameter in global sea-level changes, and has been acknowledged as the primary cause of Cretaceous sea-level highstand [*Vail et al.*, 1977; *Berner*, 1994; *Hardenbol et al.*, 1998]. Furthermore, the seafloor generation rate is thought to be a critical parameter for scaling the CO_2 outgassing rate both from the mantle and subduction metamorphism [*Berner et al.*, 1983; *Berner*, 1994].

[3] Two recent studies, both based on the more modern database of global ocean isochrons of *Royer et al.* [1992] and *Müller et al.* [1997], obviously show that such a high rate of spreading in the Cretaceous cannot be demonstrated. In the first one, *Rowley* [2002] suggests a steady state in production at 3.4 km^2 yr^{-1}, integrating the area versus age distribution of *Sclater et al.* [1981] while making the assumption of a constant consumption rate of oceanic crust at subduction zones, as proposed by *Parsons* [1981, 1982]. This idea has been recently criticized by *Demicco* [2004], who showed that a nonsteady state production of ocean crust with time may account for the observed linear decrease in area versus age of ocean floor as well. Following a different approach, we [*Cogné and Humler*, 2004] however reach the same conclusions as *Rowley* [2002]. Only on the basis of measurable elements on the Earth (surfaces and isochron lengths) we divided oceanic crust surfaces evolution with time by the length of past ridges. This led us to propose an average constant spreading half-rate of 25.9 ± 3.3 mm yr^{-1} at the global scale since at least ~160 Ma, without any significant variation in the Cretaceous. In a second and more hypothetical step, based on geological evidence [*Ricou*, 1994, *Engebretson et al.*, 1985], we modeled the temporal evolution of the length of ridges on the Earth. In quite good agreement with *Kominz* [1984], we suggest a constant ridge length in the geological past. But, in contrast to *Kominz* [1984], we conclude that constant spreading rates and ridge lengths results in a globally constant half-production rate in the past.

[4] Consequently, we face a paradox. On the one hand, *Rowley* [2002] suggests a constant oceanic crust production rate since 180 Ma, which, although debated [*Demicco*, 2004], is supported in a different way by *Cogné and Humler* [2004]. On the other hand, sea-level changes appear to be undoubtedly controlled by changes in the oceanic crust production, supposed to have a major effect in sea-level highstand in the Cretaceous [*Hays and Pitman*, 1973; *Kominz*, 1984; *Larson*, 1991]. We present here a new detailed analysis of the isochron database of *Royer et al.* [1992] and *Müller et al.* [1997], in order to provide up to date insights on temporal evolution of oceanic crust spreading (mm yr^{-1}), production (km^2 yr^{-1}) and flux (km^3 yr^{-1}) rates. Furthermore, this study is based on a recomputation of isochron ages following the recently published magnetostratigraphic scale of *Gradstein et al.* [2004b].

2. Spreading Rates (mm yr^{-1})

2.1. Method

[5] *Cogné and Humler* [2004] presented a curve of global spreading rates as a function of time, based on the average of 4 main oceanic basins (Atlantic, Indian, Antarctic and Pacific). This curve shows no significant variations since at least ~160 Ma. However, because it averages large oceanic basins, within which there may be some significant variations, one may suggest that such a simple arithmetic average could smooth periods of high (or low) spreading rates intervening on large (or small) ridge lengths.

[6] For example, it is particularly obvious that the isochron pattern of the southeastern part of the Indian Ridge system separating the Antarctica and Australia plates reflects quite high spreading rates since the Tertiary, whereas these rates are much lower in the southwestern part at the same time. Similarly, the central part of the Indian Ridge system had very high spreading rates at the time of rapid northward drift of India Plate at the end of the Cretaceous [e.g., *Patriat and Achache*, 1984] while it was rotating away from Antarctica. The rates on this ridge segment then dramatically slowed after the collision of India with Eurasia continent at ~50 Ma. Because of this complexity, averaging spreading rates at the scale of the entire Indian ridge system (as we did in our first evaluation) possibly smoothes these local variations [e.g., *Cogné and Humler*, 2004, Figure 3b]. Turning to the Atlantic Ridge system, although isochron paths appear more regular, we may suspect different behavior of its northern, central and southern parts since their histories are not synchronous. We therefore attempted to refine our evaluation of average spreading rates at the global scale by a more detailed study of rates and ridge lengths at the scale of smaller and better defined oceanic units, with more symmetric shapes than in our first evaluation.

[7] Keeping in mind the sake of symmetry and regular isochron structure, we have selected 8 oceanic units, representing ~70% of the total oceanic crust surface, in the following way (Figure 1). We selected three main parts in the Atlantic ocean: (1) the Central Atlantic basin (CATL, Figure 1a) which we arbitrarily limited to the Charlie Gibbs fracture zone (f.z.) to the north, and the Romanche f.z. to the south, thus delineating the oceanic crust formed during the rotation of North America plate from Africa since 180 Ma; (2) the South Atlantic basin (SATL, Figure 1b) which we limited to the same Romanche f.z. to the north, and the Falkland-Agulhas f.z. to the south, encompassing most of the oceanic crust generated by the rotation of South America from Africa; (3) the North Atlantic basin (NATL, Figure 1c) defined by the isochrons recorded during rotation of North America from Europe, north of the Charlie Gibbs f.z. We have not considered southernmost parts, south of the Falkland-Agulhas f.z., because of interactions between South Atlantic, Southwest Indian and South America/Antarctica ridges, including the Scotia plate.

[8] In the same way, we have divided the Indian ocean into four distinct units. (1) A western part centered on the Southwest Indian Ridge (SWIR, Figure 1e), which we limited to the Shaka f.z. to the west and the Andrew Baine f.z. to the east, encompassing the crust generated between Antarctica and Africa. (2) We considered the Somalia Basin (SB, Figure 1f) as a single (and the smallest) unit, which opened when Madagascar, together with Australia, India and Antarctica, rotated away from South Africa between ~160 and ~120 Ma. (3) The eastern part is defined between the St Paul (west) and Balleny (east) f.z., on the Southeast Indian Ridge (SEIR, Figure 1h), which generated the crust formed during rotation of Antarctica away from Australia. (4) The remaining of the Indian ocean has been considered as the Central Indian Ocean unit (CIO, Figure 1g). Indeed, the latter unit is not very simple and symmetrical, as it contains some parts of SWIR and SEIR units, but it also contains the most significant part of the crust generated at the end of the Cretaceous by the northward drift of India plate, and is therefore assumed to be significant of the Central Indian ridge dynamics.

[9] Finally, the Pacific Plate (PAC, Figure 1d) is the 8th oceanic unit we considered. It should be noted that it is the only oceanic unit which is bounded on a side by a ridge, whereas the seven other units are symmetrical relative to their ridge axis. Finally, we did not consider Nazca and Cocos plates because they are significantly subducted.

[10] In each of these oceanic units, we have computed the spreading rates SR_i (i = 1, 8 *basins*), as described by *Cogné and Humler* [2004], using *Cogné* [2003], by (1) measuring the surface dA encompassed between two successive pairs of isochron, (2) dividing these dA by the time interval dt between these isochrons, and (3) dividing these $\{dA/dt\}$ quantities by the relevant isochron length RL_i, which is the ridge remnant responsible for the dA production considered (Table 1). An error analysis is also provided which is based on [e.g., *Cogné and Humler*, 2004] a ±3% error on measured dA quantities, an assumed average 1 Myr error on isochron boundaries resulting in a $\pm 2^{0.5}$ Myr error on dt, and a 7% error on RL measurements.

[11] Finally, we recall that the isochrons were dated by *Royer et al.* [1992] and *Müller et al.* [1997] using the magnetostratigraphic scales of *Cande and Kent* [1995] for anomalies younger than chron 34 (83.5 Ma), and of *Gradstein et al.* [1994] for older periods. In the present study, we have made computations according to these references (as in *Cogné and Humler* [2004]), as well as with the recent magnetostratigraphic scale published by *Gradstein et al.* [2004a, 2004b]. We detail here only the results obtained with isochron ages which we have redated using the more recent timescale of *Gradstein et al.* [2004b].

2.2. Results

[12] The spreading rates here obtained are shown in Figure 2 (full rates). They show great variability between oceans. Spreading rates appear particularly regular in the Central Atlantic basin (Figure 2a) at an average value of 28.3 ± 7.8 mm yr^{-1}, whereas they show significant variations in the South Atlantic ocean, with high values (50 mm yr^{-1}) during the Cretaceous, and in the ~20–40 Ma period (~45 mm yr^{-1}), with lower (30 to 40 mm yr^{-1}) in the 70–50 and 20–0 Ma periods. Because it is close to the Euler pole of rotation between North America and Europe, the North Atlantic unit provides lower and quite constant spreading rates (Figure 2c) which average at 19.8 ± 6.0 mm yr^{-1} since 80 Ma. However, the greater variability appears in the Indian Ocean, and in the Pacific. Concerning the Indian Ocean, it is upsetting to observe that each of its three main parts exhibits high spreading rates periods which become younger from west to east. As a matter of fact, the SWIR

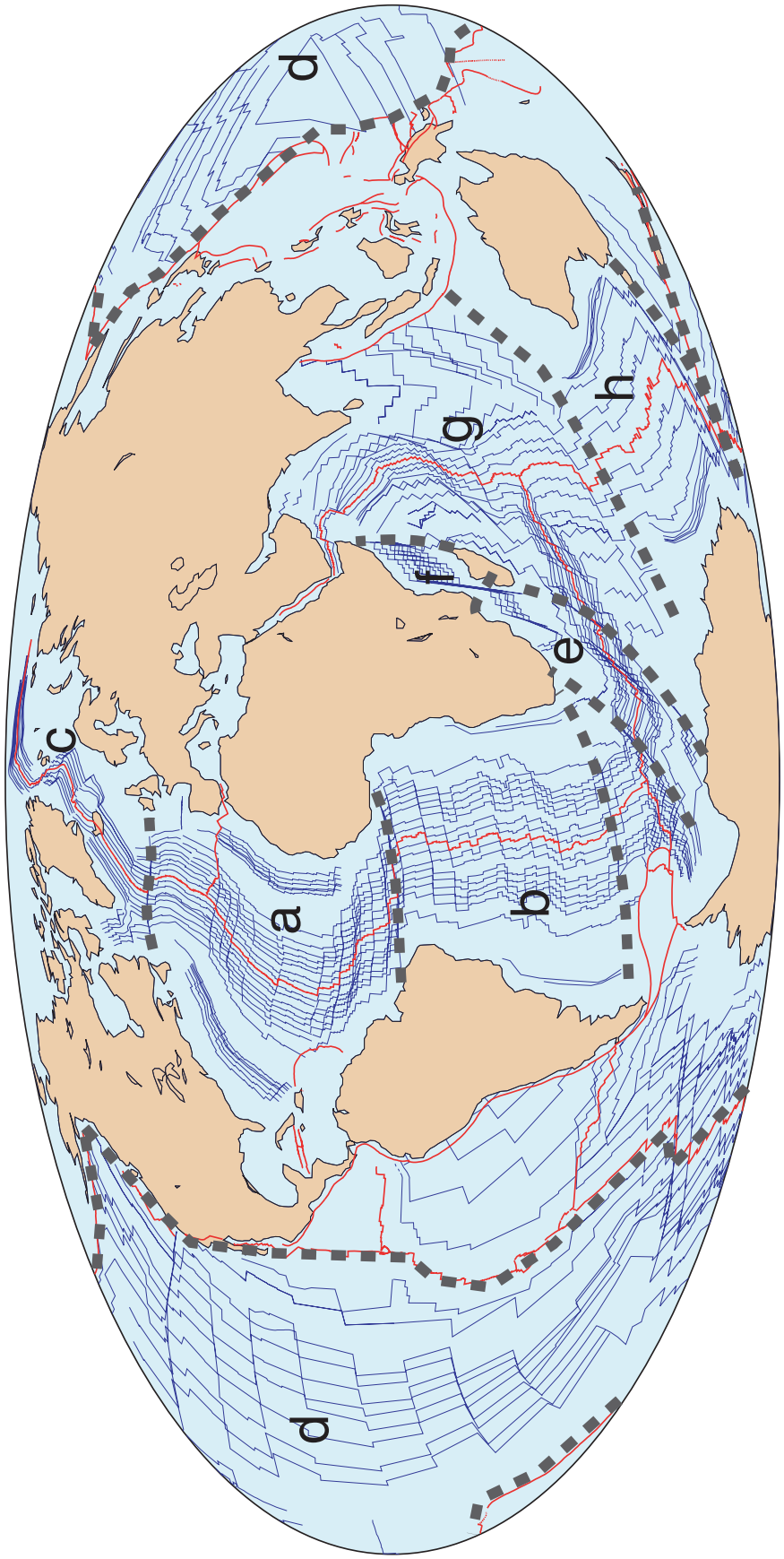

Figure 1. Hammer-Aitoff projection of isochrons (blue thin lines) based on *Royer et al.* [1992] and *Müller et al.* [1997] and definition of the 8 oceanic units we have selected for our new computation of spreading rates: (a) Central Atlantic (CATL), (b) South Atlantic (SATL), (c) North Atlantic (NATL) (d) Pacific plate (PAC), (e) Southwest Indian Ridge (SWIR), (f) Somalia Basin (SB), (g) Central Indian Ocean (CIO), and (h) Southeast Indian Ridge (SEIR). Limits between the units are drawn as bold hatched lines.

Table 1. Seafloor Spreading Data (Full Rates) as Computed From Isochrons 0 to M25 for the 8 Oceanic Units Considered[a]

Chron	t, Ma	dA/dt, km^2/yr	Ridge Length (RL), km	Spreading Rate (SR), mm/yr
		Central Atlantic (CATL)		
0	0.0	0.182 ± 0.021	6319.2 ± 442.3	28.8 ± 3.1
5	9.8	0.172 ± 0.019	6171.0 ± 432.0	27.8 ± 2.9
6	19.7	0.164 ± 0.012	6132.8 ± 429.3	26.8 ± 1.9
13	33.3	0.205 ± 0.041	5888.0 ± 412.2	34.8 ± 6.4
18	39.5	0.187 ± 0.028	5950.2 ± 416.5	31.5 ± 4.4
21	47.2	0.190 ± 0.023	6197.7 ± 433.8	30.7 ± 3.4
25	56.7	0.166 ± 0.016	6301.5 ± 441.1	26.3 ± 2.4
31	67.8	0.200 ± 0.012	5985.1 ± 419.0	33.4 ± 1.9
34	83.5	0.174 ± 0.001	6320.9 ± 442.5	27.6 ± 0.1
M0	124.6	0.112 ± 0.027	6164.9 ± 431.5	18.1 ± 4.1
M4	129.8	0.046 ± 0.012	3457.7 ± 242.0	13.2 ± 3.2
M10	134.6	0.080 ± 0.013	3305.6 ± 231.4	24.1 ± 3.6
M16	142.1	0.094 ± 0.018	3337.8 ± 233.6	28.1 ± 4.9
M21	148.5	0.155 ± 0.035	3196.8 ± 223.8	48.5 ± 10.2
M25	154.1	0.079 ± 0.002	3128.5 ± 219.0	25.3 ± 0.6
>M25	180.0			
		South Atlantic (SATL)		
0	0.0	0.210 ± 0.024	5152.6 ± 360.7	40.8 ± 1.8
5	9.8	0.215 ± 0.024	5199.2 ± 363.9	41.4 ± 1.7
6	19.7	0.250 ± 0.019	5188.7 ± 363.2	48.1 ± 0.2
13	33.3	0.280 ± 0.055	5296.9 ± 370.8	52.9 ± 6.8
18	39.5	0.226 ± 0.034	5254.2 ± 367.8	43.1 ± 3.5
21	47.2	0.168 ± 0.020	5328.0 ± 373.0	31.6 ± 1.6
25	56.7	0.160 ± 0.016	5291.9 ± 370.4	30.2 ± 0.8
31	67.8	0.293 ± 0.018	5277.5 ± 369.4	55.4 ± 0.5
34	83.5	0.235 ± 0.001	5213.1 ± 364.9	45.2 ± 3.0
M0	124.6	0.088 ± 0.022	3338.3 ± 233.7	26.4 ± 4.6
M4	129.8	0.099 ± 0.026	2050.7 ± 143.6	48.3 ± 9.2
M10	134.6			
		North Atlantic (NATL)		
0	0.0	0.104 ± 0.012	5717.6 ± 400.2	18.2 ± 0.8
5	9.8	0.067 ± 0.008	5481.2 ± 383.7	12.3 ± 0.5
6	19.7	0.063 ± 0.005	4987.2 ± 349.1	12.6 ± 0.1
13	33.3	0.119 ± 0.024	4385.1 ± 307.0	27.2 ± 3.5
18	39.5	0.112 ± 0.017	4448.3 ± 311.4	25.2 ± 2.1
21	47.2	0.096 ± 0.012	5772.6 ± 404.1	16.6 ± 0.8
25	56.7	0.026 ± 0.003	987.9 ± 69.2	26.6 ± 0.7
31	67.8	0.019 ± 0.001	944.1 ± 66.1	19.8 ± 0.2
34	83.5			
		Pacific Plate (PAC)[b]		
0	0.0	0.856 ± 0.149	12143.4 ± 850.0	140.9 ± 34.5
5	9.8	0.521 ± 0.090	12957.0 ± 907.0	80.4 ± 19.5
6	19.7	0.876 ± 0.118	14273.5 ± 999.1	122.7 ± 25.1
13	33.3	0.571 ± 0.147	15598.8 ± 1091.9	73.2 ± 24.0
18	39.5	0.646 ± 0.137	15430.1 ± 1080.1	83.7 ± 23.6
21	47.2	0.514 ± 0.093	15005.0 ± 1050.3	68.5 ± 17.1
25	56.7	0.524 ± 0.082	16523.5 ± 1156.6	63.4 ± 14.4
31	67.8	0.544 ± 0.065	16294.8 ± 1140.6	66.8 ± 12.7
34	83.5	0.567 ± 0.037	13287.8 ± 930.1	85.4 ± 11.5
M0	124.6	0.446 ± 0.136	4724.2 ± 330.7	188.7 ± 70.7
M4	129.8	0.375 ± 0.120	7623.5 ± 533.6	98.4 ± 38.5
M10	134.6	0.390 ± 0.086	6466.9 ± 452.7	120.6 ± 35.0
M16	142.1	0.437 ± 0.109	7892.1 ± 552.4	110.8 ± 35.3
M21	148.5	0.391 ± 0.112	7707.8 ± 539.5	101.5 ± 36.1
M25	154.1	0.234 ± 0.020	7250.5 ± 507.5	64.7 ± 10.0
>M25	180.0			

Table 1. (continued)

Chron	t, Ma	dA/dt, km^2/yr	Ridge Length (RL), km	Spreading Rate (SR), mm/yr
		Southwest Indian Ridge (SWIR)		
0	0.0	0.031 ± 0.004	1621.7 ± 113.5	19.1 ± 0.9
5	9.8	0.024 ± 0.003	1700.5 ± 119.0	14.2 ± 0.6
6	19.7	0.036 ± 0.003	1641.7 ± 114.9	21.9 ± 0.1
13	33.3	0.043 ± 0.009	1393.6 ± 97.6	31.1 ± 4.0
18	39.5	0.037 ± 0.006	1521.8 ± 106.5	24.2 ± 2.0
21	47.2	0.030 ± 0.004	1724.4 ± 120.7	17.5 ± 0.9
25	56.7	0.036 ± 0.004	2260.5 ± 158.2	16.1 ± 0.4
31	67.8	0.085 ± 0.005	2147.3 ± 150.3	39.4 ± 0.4
34	83.5	0.079 ± 0.000	1303.1 ± 91.2	60.6 ± 4.0
M0	124.6	0.044 ± 0.011	1167.7 ± 81.7	38.0 ± 6.6
M4	129.8	0.036 ± 0.010	825.3 ± 57.8	44.1 ± 8.4
M10	134.6	0.033 ± 0.005	807.0 ± 56.5	40.9 ± 3.7
M16	142.1	0.048 ± 0.009	812.0 ± 56.8	59.1 ± 7.0
M21	148.5	0.069 ± 0.006	815.3 ± 57.1	84.9 ± 2.0
>M21	160.0			
		Somalia Basin (SB)		
-	*~120*	0.017 ± 0.005	930.2 ± 65.1	17.8 ± 3.7
M0	124.6	0.038 ± 0.009	930.2 ± 65.1	40.9 ± 7.1
M4	129.8	0.030 ± 0.008	891.3 ± 62.4	34.0 ± 6.5
M10	134.6	0.038 ± 0.006	893.0 ± 62.5	42.9 ± 3.9
M16	142.1	0.049 ± 0.009	924.6 ± 64.7	53.0 ± 6.3
M21	148.5	0.060 ± 0.006	849.2 ± 59.4	70.5 ± 1.6
>M21	160.0			
		Central Indian Ocean (CIO)		
0	0.0	0.358 ± 0.041	10023.3 ± 701.6	35.7 ± 1.6
5	9.8	0.346 ± 0.039	9682.0 ± 677.7	35.7 ± 1.5
6	19.7	0.291 ± 0.022	10078.8 ± 705.5	28.9 ± 0.1
13	33.3	0.286 ± 0.057	8113.5 ± 567.9	35.2 ± 4.5
18	39.5	0.253 ± 0.039	6758.8 ± 473.1	37.5 ± 3.1
21	47.2	0.504 ± 0.060	6213.8 ± 435.0	81.1 ± 4.1
25	56.7	0.659 ± 0.064	6055.6 ± 423.9	108.9 ± 2.9
31	67.8	0.293 ± 0.018	3982.7 ± 278.8	73.5 ± 0.7
34	83.5	0.147 ± 0.001	3481.5 ± 243.7	42.1 ± 2.8
M0	124.6			
		Southeast Indian Ridge (SEIR)		
0	0.0	0.360 ± 0.041	4736.4 ± 331.5	76.0 ± 3.4
5	9.8	0.288 ± 0.032	4821.3 ± 337.5	59.6 ± 2.5
6	19.7	0.338 ± 0.025	4946.2 ± 346.2	68.2 ± 0.3
13	33.3	0.256 ± 0.051	4573.8 ± 320.2	56.0 ± 7.2
18	39.5	0.143 ± 0.022	4810.2 ± 336.7	29.8 ± 2.4
21	47.2	0.029 ± 0.003	3592.0 ± 251.4	8.1 ± 0.4
25	56.7	0.016 ± 0.002	3480.4 ± 243.6	4.7 ± 0.1
31	67.8	0.028 ± 0.002	3422.7 ± 239.6	8.2 ± 0.1
34	83.5	0.017 ± 0.000	3345.0 ± 234.1	5.1 ± 0.3
M0	124.6			

[a] Notes: t, age of the isochrons after *Gradstein et al.* [2004b]; dA/dt, area per unit age.
[b] SR values for Pacific have been doubled for comparison with other basins.

(Figure 2e) shows high spreading rates (with important fluctuations around ~75 mm yr^{-1}) at the beginning of its life, from 155 to 83 Ma, where it falls by more than 50%, and then remains stable up to the present-day period. The SB spreading rates (Figure 2f) are in line with those of SWIR in the ~125–160 Ma period. The SWIR decrease of spreading rate is followed by an increase of the Central Indian Ocean one (Figure 2g) which reaches twice its initial value at ~100 mm yr^{-1} between 70 and 50 Ma, the time of rapid northward drift of India plate, and then decreases to a stable value of ~35 mm yr^{-1}. Corresponding to this decrease at 50 Ma, the SEIR (Figure 2h) shows an increase of spreading rates between 50 and 35 Ma where it reaches ~65 mm yr^{-1} whereas it

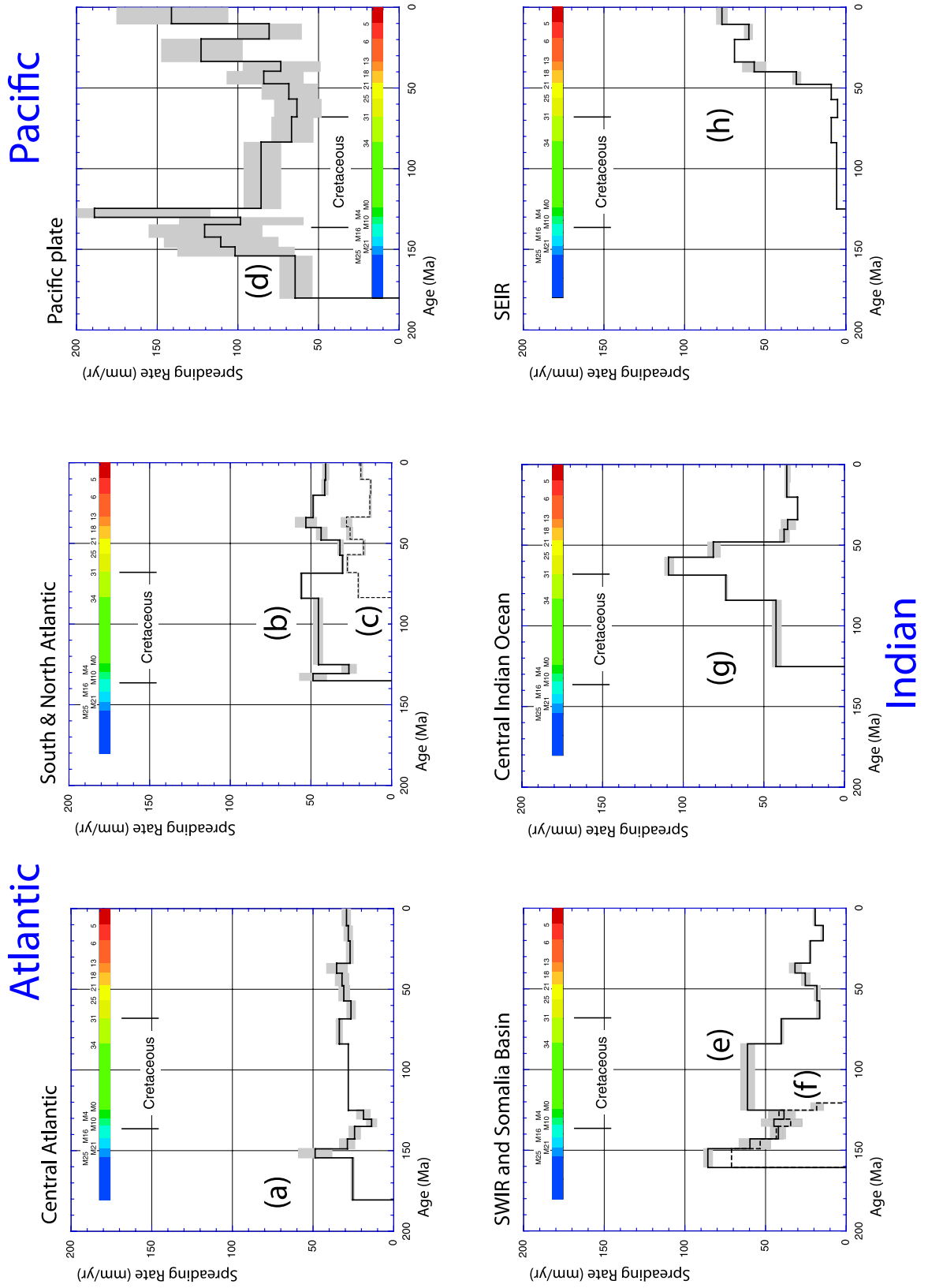
Atlantic
Pacific
Indian
Central Atlantic
South & North Atlantic
Pacific plate
SEIR
SWIR and Somalia Basin
Central Indian Ocean
Cretaceous
(a)
(b)
(c)
(d)
(e)
(f)
(g)
(h)
Spreading Rate (mm/yr)
Age (Ma)
0
50
100
150
200
M25 M21 M16 M10 M4 M0
34 31 25 21 18 13 6 5

Figure 2

Table 2. Weighting Factors and Weighted Spreading Rate (Full-Rate) Computed After the Data of Table 1[a]

Chron	t, Ma	CATL	SATL	NATL	PAC	SWIR	SB	CIO	SEIR	Weighted SR, mm/yr
0	0.0	0.138	0.113	0.125	0.266	0.035	-	0.219	0.104	64.7 ± 9.2
5	9.8	0.134	0.113	0.119	0.282	0.037	-	0.210	0.105	46.8 ± 5.5
6	19.7	0.130	0.110	0.106	0.302	0.035	-	0.213	0.105	61.2 ± 7.6
13	33.3	0.130	0.117	0.097	0.345	0.031	-	0.179	0.101	51.5 ± 8.4
18	39.5	0.135	0.119	0.101	0.349	0.034	-	0.153	0.109	50.9 ± 8.3
21	47.2	0.141	0.122	0.132	0.342	0.039	-	0.142	0.082	46.7 ± 5.9
25	56.7	0.154	0.129	0.024	0.404	0.055	-	0.148	0.085	51.6 ± 5.8
31	67.8	0.157	0.139	0.025	0.428	0.056	-	0.105	0.090	52.7 ± 5.4
34	83.5	0.192	0.158	-	0.403	0.040	-	0.106	0.102	54.2 ± 4.7
M0	124.6	0.378	0.204	-	0.289	0.072	0.057	-	-	73.8 ± 21.8
M4	129.8	0.233	0.138	-	0.513	0.056	0.060	-	-	66.7 ± 21.1
M10	134.6	0.288	-	-	0.564	0.070	0.078	-	-	84.3 ± 21.4
M16	142.1	0.257	-	-	0.609	0.063	0.071	-	-	84.4 ± 23.2
M21	148.5	0.254	-	-	0.613	0.065	0.068	-	-	85.9 ± 23.9
M25	154.1	0.301	-	-	0.699	-	-	-	-	52.8 ± 7.0
>M25	180.0									

[a] Weighting factors computed as (Ridge Length/Total Ridge Length); Weighted SR, global weighted spreading rate; oceanic unit abbreviations as in Table 1.

evolved very slowly between 122 and 50 Ma at 5–10 mm yr^{-1}.

[13] The Pacific plate is bounded on its eastern side by a ridge and thus the *SR* values have been doubled (Table 1) for comparison with other, symmetric, basins. As usually noted, Pacific rates are almost twice as large as rates from the other basins. They show high values between 180 and 83 Ma, at ~100 mm yr^{-1}, followed by a decrease to ~65 mm yr^{-1} between 83 and 40 Ma, and an increase in the 40 last Myr to their present-day values of 120–140 mm yr^{-1}.

[14] Because the spreading rates just described apply to various ridge lengths, with possibly high rates on only short ridge segments, or low rates involving long ridge segments, we propose to weight the global average to ridge length. We therefore computed weights wt_i (i = 1, 8) as the ratio of a given ridge length SR_i for a given oceanic basin at a given age with the total ridge length we could measure for this age on the whole 8 oceanic units considered (Table 2). The weighted global average spreading rates we propose (Table 2, Figure 3a) are then assumed to be the sum of the products $\{SR_i.wt_i\}$ (i = 1, 8) from 180 Ma to present.

[15] The weighted average spreading rates (Table 2, Figure 3a) appear quite consistent with our previous determination [*Cogné and Humler*, 2004] and constant at 53.4 ± 5.9 (1σ) mm yr^{-1} through the 125–0 Ma period. Although they appear consistent in the last 50 Myr, our results are significantly lower than both lower (green curve in Figure 3a) and higher (blue curve) hypotheses of *Kominz* [1984] prior to 50 Ma. The reasons for this discrepancy, as already discussed by *Cogné and Humler* [2004], are thought to arise from (1) different methods, (2) improved mapping of isochrons, and (3) a better accuracy of timescales used since the time of the latter evaluation. The procedure adopted here further allows us to significantly reduce the 2σ errors with respect to our previous determination (e.g., dark versus light gray areas in Figure 3a). This reinforces the hypothesis of the lack of significant high spreading rates on ridges during most of the Cretaceous.

[16] In contrast with our previous study, however, the present results suggest higher spreading rates prior to anomaly M0, which would average at 77.0 ± 8.4 (1σ) mm yr^{-1} between M25 (148.5 Ma) and M0 (124.6 Ma). It should however be noted that (1) the average spreading rates are dominated by the high Pacific values, as they represent ~50% of the total ridge length measured at the time of anomaly M4 (Table 2), and up to 70% prior to M21. In contrast, *SR* values of Somalia Basin, SWIR and Central Atlantic appear lower, around

Figure 2. Spreading rates (mm yr^{-1}) as a function of time, computed as $\{dA/dt\}/RL$ for each of the 8 oceanic basins considered; (a – h) as in Figure 1. The color scales represent chrons 0, 5, 6, 13, 18, 21, 25, 31, 34, M0, M4, M10, M16, M21, and M25 with their ages in Ma, following the geomagnetic timescale of *Gradstein et al.* [2004b]; all the plots are at the same scale.

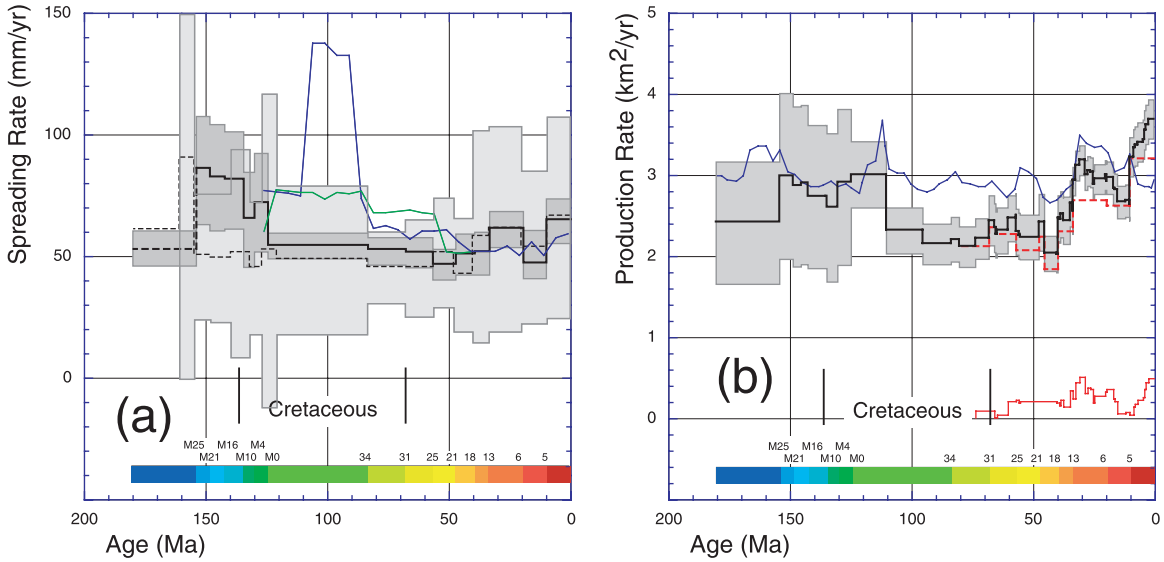

Figure 3. (a) Continuous black curve and dark gray area: weighted average spreading rates (full rates in mm yr^{-1}) and 2σ error area as a function of time for the present study; blue (green) curve: higher (lower) hypothesis of *Kominz* [1984]; dotted black curve and light gray area following *Cogné and Humler* [2004]. (b) Global oceanic crust production rates (km^2 yr^{-1}) as a function of time; continuous black line and gray area: total production rates with 2σ error including back arc basins deduced from *Kaiho and Saito* [1994] (red continuous curve); red dotted line: production at main ridges only, after *Cogné and Humler* [2004], corrected for the timescale of *Gradstein et al.* [2004b]; blue curve: following *Rowley* [2002].

25–50 mm yr^{-1} in the same period (Table 1, Figure 2). (2) Surfaces enclosed by (and older than) the M0 anomaly represent only ~13% of the total measured surfaces on the Earth. Therefore spreading rates determinations are sensitive to small errors on either *dA* or *dt* quantities. Altogether, we conclude that the high spreading rates we propose for periods older than 125 Ma are probably speculative.

3. Production Rates (km^2 yr^{-1})

[17] The production rate we present here relies on the same assumptions as of *Cogné and Humler* [2004]. It is based on the sum of currently observable surface production rates $\{dA/dt\}$ at the global scale, as first compiled by *Sclater et al.* [1981] and refined by *Rowley* [2002] and *Cogné and Humler* [2004], with the $\{dA/dt\}$ of subducted, oceanic crust. To obtain this modeled production, we computed the product of ridge lengths of *Cogné and Humler* [2004], based on Tethys and Pacific model evolutions [*Ricou*, 1994; *Engebretson et al.*, 1985], with the weighted global spreading rates as quoted above (Table 2). For the uncertainty analysis, we allowed a 15% error on estimated ridge lengths from the Pacific system, and assumed a 20% error on Tethys ones. Furthermore, we added to this production rate those of small oceanic basins (SOB) as deduced from the review of oceanic crust flux of *Kaiho and Saito* [1994], by dividing their values of crust flux in back arc basins (km^3 yr^{-1}) by the constant 6.5 km thickness they used (red curve in Figure 3b).

[18] The curve of production rates as a function of time from 180 Ma to present obtained (Table 3, Figure 3b) is very similar to the one we proposed, neglecting SOB [*Cogné and Humler*, 2004]. As already reported by *Rowley* [2002] and *Cogné and Humler* [2004], the production rates exhibit ±25% variations around a mean of 2.7 ± 0.2 km^2 yr^{-1}, with no particular high rates in the Cretaceous. In contrast, we propose that the 100–40 Ma interval might be a period of slightly lower production, somewhat contradicting the result of *Rowley* [2002] (blue curve in Figure 3b). However, the more surprising feature is a significant increase in crust production during the last 50 Myr. As a matter of fact, the average production at main ridges only (dotted red curve in Figure 3b) in the 95–56.6 Ma period establishes at 2.2 ± 0.1 km^2 yr^{-1}, whereas it is now at 3.2 ± 0.2 km^2 yr^{-1} (Table 3), an increase of 45% since 50 Ma. The total production curve (black continuous

Table 3. Oceanic Crust Production

Chron	t, Ma	Ridges dA/dt, km^2/yr	Back Arc dA/dt,[a] km^2/yr	Total dA/dt, km^2/yr
0	0.0	3.194 ± 0.241	0.492	3.685 ± 0.241
	2.4	" "	0.428	3.622 ± 0.241
	3.6	" "	0.359	3.553 ± 0.241
	4.1	" "	0.248	3.442 ± 0.241
	4.6	" "	0.214	3.407 ± 0.241
	6.5	" "	0.172	3.366 ± 0.241
	7.6	" "	0.141	3.334 ± 0.241
	8.6	" "	0.027	3.221 ± 0.241
5	9.8	2.610 ± 0.202	"	2.637 ± 0.202
	10.2	" "	0.067	2.677 ± 0.202
	11.8	" "	0.051	2.660 ± 0.202
	15.0	" "	0.209	2.819 ± 0.202
	15.9	" "	0.227	2.837 ± 0.202
	16.9	" "	0.359	2.969 ± 0.202
	19.4	" "	0.312	2.922 ± 0.202
6	19.7	2.681 ± 0.181	"	2.993 ± 0.181
	20.3	" "	0.265	2.945 ± 0.181
	24.4	" "	0.192	2.873 ± 0.181
	24.9	" "	0.352	3.032 ± 0.181
	26.3	" "	0.372	3.052 ± 0.181
	27.4	" "	0.309	2.990 ± 0.181
	28.4	" "	0.497	3.178 ± 0.181
	30.5	" "	0.429	3.109 ± 0.181
	32.5	" "	0.242	2.923 ± 0.181
13	33.2	2.303 ± 0.284	"	2.545 ± 0.284
	33.3	" "	0.341	2.644 ± 0.284
	34.4	" "	0.137	2.440 ± 0.284
	37.0	2.298 ± 0.284	"	2.434 ± 0.284
	37.2	" "	0.216	2.514 ± 0.284
	38.2	" "	0.157	2.455 ± 0.284
	39.1	" "	0.176	2.473 ± 0.284
18	39.5	1.839 ± 0.210	"	2.015 ± 0.210
	40.2	" "	0.193	2.032 ± 0.210
	45.0	2.209 ± 0.343	"	2.402 ± 0.343
21	47.2	2.045 ± 0.273	0.193	2.238 ± 0.273
	55.3	" "	0.180	2.225 ± 0.273
	55.7	" "	0.224	2.269 ± 0.273
25	56.7	2.274 ± 0.284	"	2.498 ± 0.284
	56.7	" "	0.196	2.471 ± 0.284
	60.0	" "	0.042	2.316 ± 0.284
	64.2	" "	0.000	2.274 ± 0.284
	65.0	2.356 ± 0.305	"	2.356 ± 0.305
	65.8	" "	0.091	2.447 ± 0.305
31	67.8	2.132 ± 0.252	"	2.222 ± 0.252
	73.4	" "	0.000	2.132 ± 0.252
	80.0	2.215 ± 0.275	"	2.215 ± 0.275
34	83.5	2.149 ± 0.249	"	2.149 ± 0.249
	95.0	2.320 ± 0.281	"	2.320 ± 0.281
	110.0	3.004 ± 0.411	"	3.004 ± 0.411
M0	124.6	2.852 ± 0.971	"	2.852 ± 0.971
M4	129.8	2.604 ± 0.912	"	2.604 ± 0.912
M10	134.6	2.739 ± 0.886	"	2.739 ± 0.886
	135.0	2.731 ± 0.880	"	2.731 ± 0.880
M16	142.1	2.897 ± 0.972	"	2.897 ± 0.972
	145.0	2.861 ± 0.989	"	2.861 ± 0.989
M21	148.5	2.990 ± 1.030	"	2.990 ± 1.030
M25	154.1	2.418 ± 0.752	"	2.418 ± 0.752
>M25	180.0			

[a] After *Kaiho and Saito* [1994].

curve in Figure 3b), including SOB production, indeed exhibits a larger increase of production, on the order of 60%, with 2.3 ± 0.1 km^2 yr^{-1} in the 95–56.6 Ma period and 3.7 ± 0.2 km^2 yr^{-1} at present.

[19] As noted by *Kaiho and Saito* [1994], there are some significant variations in the production of back arc basins at the global scale, with high values within 0–7 Ma, 15–34 Ma and 37–60 Ma periods, and low values within 8–15 Ma, 34–37 Ma and 60–66 Ma periods. These variations fit the trends of production rates we see in the main oceanic basins (red dotted line in Figure 3b), with high values between chrons 0 and 5 (0–9.8 Ma), 6 and 13 (19.7–33.3 Ma) and possibly 21 and 31 (47.2–67.8 Ma), and relatively lower values between chrons 5 and 6 (9.8–19.7 Ma) and 13 and 21 (33.3–47.2 Ma). As a consequence, adding SOB to main oceanic basins production measured enhances these variations and results in a possible pseudo-periodicity of ~25 Myr of crust production during the last 75–80 Myr, with fluctuations of the order of ± 0.5 km^2 yr^{-1} superposed to the general increasing trend since ~50 Ma (Figure 3b).

[20] We finally note that these pseudo-periodic variations are consistent with the curve of *Rowley* [2002], mainly in the 0–80 Ma period, but also probably in periods older than 110 Ma (Figure 3b). In contrast, however, the production rates we obtain are significantly lower than those of *Rowley* [2002] in the 110–40 Ma period (Figure 3b), although both studies are based on the same isochron database. This difference might arise from different methods used. In effect, *Rowley* [2002] chose to integrate the $\{dA/dt\}$ distribution, making the strong hypothesis of a regular triangular distribution [e.g., *Sclater et al.*, 1981] resulting from regular production through times, and age-independent subduction of oceanic lithosphere [*Parsons*, 1981, 1982]. These hypotheses led the author to advocate a steady-state model of ocean floor production. Recently, *Demicco* [2004] showed that the observed linear decrease in area versus age of ocean floor does not force a steady-state view of seafloor production, which we do not observe following the method described above.

4. Oceanic Crust Flux Rates (km^3 yr^{-1})

[21] In the following, flux rate is the total amount, in volume (km^3 yr^{-1}), of produced crust in the last 180 Myr. We therefore have to envision two main aspects which are (1) the flux at ridges which may vary as a function of mantle temperature variations, as suggested by *Humler et al.* [1999], and (2) the total volume of oceanic plateaus as proposed by *Larson* [1991] and *Hardebeck and Anderson* [1996]. Accounting for the first aspect of the question, assuming a constant mantle temperature would provide a constant thickness of crust generation in volume, and consists in multiplying our production rates (Table 3) by a constant thickness. Assuming a constant thickness at ridges of 7 km, one obtains an evolution of crustal flux at ridges which, indeed, does not differ from the production curve in surfaces (Table 4; dotted line in Figure 4a). This minimum hypothesis therefore provides a roughly constant flux rate through times, with an average of 18.7 ± 2.9 km^3 yr^{-1}. This value is in fairly good agreement with the generally accepted production at ridges of ~20 km^3 yr^{-1} [e.g., *Anderson*, 1974; *Schilling et al.*, 1978; *Wilson*, 1989].

[22] A second, and valid, hypothesis is to add to this production, the effect of mantle temperature variations. Following *Klein and Langmuir* [1987], *Langmuir et al.* [1992], and *Humler et al.* [1993], the chemical composition (major and trace elements) of oceanic crust basalts can be quantitatively linked to mantle temperature at the time of effusion. An investigation of ancient crustal composition of Atlantic, Pacific and Indian oceans allowed *Humler et al.* [1999] to show that the mantle temperature was probably hotter by 50°C prior to 80 Ma, whereas it is, on average, identical to present-day values since then. On the other hand, the amount of melt in the mantle beneath an oceanic ridge is controlled by the amount of pressure release that each individual parcel of mantle has experienced [e.g., *Klein and Langmuir*, 1987; *Langmuir et al.*, 1992]. The higher the mantle temperature, the more melt produced, and hence the greater the thickness of the oceanic crust [e.g., *McKenzie*, 1984]. Regardless of the origin of mantle temperature variations [*Humler and Besse*, 2002; *Machetel and Humler*, 2003] the chemical data suggest that crustal thicknesses were 1–2 km thicker before 80 Ma (~9 km) than at present (~7 km [e.g., *Humler et al.*, 1999; *Cogné and Humler*, 2004]). We therefore present a second model, where the flux rates are computed as the product of the production rates of Table 3 by a 7 km thickness from 80 Ma to present, and 9 km before 80 Ma (Table 4, continuous line in Figure 4a). This curve should therefore represent the crustal flux at ridges in the hypothesis of a 50°C thermal jump in the mantle at 80 Ma. It shows the main features we observed in production rates, and in particular the increase in crust flux rate in the last 50 Myr

Table 4. Oceanic Crust Flux

Chron	t, Ma	Plateaus,[a] km^3/yr	Back Arc,[b] km^3/yr	Main Basins,[c] km^3/yr		Ridges (Main Basins + Back Arc),[d] km^3/yr		Total (Ridges + Plateaus),[e] km^3/yr	
				No Thermal Jump (80 Ma)	Thermal Jump (80 Ma)	No Thermal Jump (80 Ma)	Thermal Jump (80 Ma)	No Thermal Jump (80 Ma)	Thermal Jump 80 Ma)
0	0.0	1.5	3.2	22.4 ± 1.7	22.4 ± 1.7	25.5	25.5	27.0	27.0
	2.4	"	2.8	" "	" "	25.1	25.1	26.6	26.6
	3.6	"	2.3	" "	" "	24.7	24.7	26.2	26.2
	4.1	"	1.6	" "	" "	24.0	24.0	25.5	25.5
	4.6	"	1.4	" "	" "	23.7	23.7	25.2	25.2
	6.5	"	1.1	" "	" "	23.5	23.5	25.0	25.0
	7.6	"	0.9	" "	" "	23.3	23.3	24.8	24.8
	8.6	"	0.2	" "	" "	22.5	22.5	24.0	24.0
5	9.8	"	"	18.3 ± 1.4	18.3 ± 1.4	18.4	18.4	19.9	19.9
	10.0	1.0	"	" "	" "	18.4	18.4	19.4	19.4
	10.2	"	0.4	" "	" "	18.7	18.7	19.7	19.7
	11.8	"	0.3	" "	" "	18.6	18.6	19.6	19.6
	15.0	"	1.4	" "	" "	19.6	19.6	20.6	20.6
	15.9	"	1.5	" "	" "	19.7	19.7	20.7	20.7
	16.9	"	2.3	" "	" "	20.6	20.6	21.6	21.6
	19.4	"	2.0	" "	" "	20.3	20.3	21.3	21.3
6	19.7	"	"	18.8 ± 1.3	18.8 ± 1.3	20.8	20.8	21.8	21.8
	20.0	0.5	"	" "	" "	20.8	20.8	21.3	21.3
	20.3	"	1.7	" "	" "	20.5	20.5	21.0	21.0
	24.4	"	1.3	" "	" "	20.0	20.0	20.5	20.5
	24.9	"	2.3	" "	" "	21.1	21.1	21.6	21.6
	26.3	"	2.4	" "	" "	21.2	21.2	21.7	21.7
	27.4	"	2.0	" "	" "	20.8	20.8	21.3	21.3
	28.4	"	3.2	" "	" "	22.0	22.0	22.5	22.5
	30.0	0.5	"	" "	" "	22.0	22.0	22.5	22.5
	30.5	"	2.8	" "	" "	21.6	21.6	22.1	22.1
	32.5	"	1.6	" "	" "	20.3	20.3	20.8	20.8
13	33.2	"	"	16.1 ± 2.0	16.1 ± 2.0	17.7	17.7	18.2	18.2
	33.3	"	2.2	" "	" "	18.3	18.3	18.8	18.8
	34.4	"	0.9	" "	" "	17.0	17.0	17.5	17.5
	37.0	"	"	16.1 ± 2.0	16.1 ± 2.0	17.0	17.0	17.5	17.5
	37.2	"	1.4	" "	" "	17.5	17.5	18.0	18.0
	38.2	"	1.0	" "	" "	17.1	17.1	17.6	17.6
	39.1	"	1.1	" "	" "	17.2	17.2	17.7	17.7
18	39.5	"	"	12.9 ± 1.5	12.9 ± 1.5	14.0	14.0	14.5	14.5
	40.0	1.5	"	" "	" "	14.0	14.0	15.5	15.5
	40.2	"	1.3	" "	" "	14.1	14.1	15.6	15.6
	45.0	1.0	"	15.5 ± 2.4	15.5 ± 2.4	16.7	16.7	17.7	17.7
21	47.2	"	"	14.3 ± 1.9	14.3 ± 1.9	15.6	15.6	16.6	16.6
	50.0	2.0	"	" "	" "	15.6	15.6	17.6	17.6
	55.0	3.0	"	" "	" "	15.6	15.6	18.6	18.6
	55.3	"	1.2	" "	" "	15.5	15.5	18.5	18.5
	55.7	"	1.5	" "	" "	15.8	15.8	18.8	18.8
25	56.7	"	"	15.9 ± 2.0	15.9 ± 2.0	17.4	17.4	20.4	20.4
	56.7	"	1.3	" "	" "	17.2	17.2	20.2	20.2
	60.0	3.5	0.3	" "	" "	16.2	16.2	19.7	19.7
	64.2	"	0.0	" "	" "	15.9	15.9	19.4	19.4
	65.0	1.5	"	16.5 ± 2.1	16.5 ± 2.1	16.5	16.5	18.0	18.0
	65.8	"	0.6	" "	" "	17.1	17.1	18.6	18.6
31	67.8	"	"	14.9 ± 1.8	14.9 ± 1.8	15.5	15.5	17.0	17.0
	70.0	1.5	"	" "	" "	15.5	15.5	17.0	17.0
	73.4	"	0.0	" "	" "	14.9	14.9	16.4	16.4
	75.0	3.5	"	" "	" "	14.9	14.9	18.4	18.4
	80.0	3.5	"	15.5 ± 1.9	19.9 2.5	15.5	19.9	19.0	23.4
34	83.5	"	"	15.0 ± 1.7	19.3 2.2	15.0	19.3	18.5	22.8
	85.0	3.5	"	" "	" "	15.0	19.3	18.5	22.8
	90.0	3.5	"	" "	" "	15.0	19.3	18.5	22.8

Table 4. (continued)

Chron	t, Ma	Plateaus,[a] km^3/yr	Back Arc,[b] km^3/yr	Main Basins,[c] km^3/yr		Ridges (Main Basins + Back Arc),[d] km^3/yr		Total (Ridges + Plateaus),[e] km^3/yr	
				No Thermal Jump (80 Ma)	Thermal Jump (80 Ma)	No Thermal Jump (80 Ma)	Thermal Jump (80 Ma)	No Thermal Jump (80 Ma)	Thermal Jump 80 Ma)
	95.0	4.0	"	16.2 ± 2.0	20.9 ± 2.5	16.2	20.9	20.2	24.9
	100.0	8.0	"	" "	" "	16.2	20.9	24.2	28.9
	105.0	6.5	"	" "	" "	16.2	20.9	22.7	27.4
	110.0	6.0	"	21.0 ± 2.9	27.0 3.7	21.0	27.0	27.0	33.0
	115.0	6.0	"	" "	" "	21.0	27.0	27.0	33.0
	120.0	6.0	"	" "	" "	21.0	27.0	27.0	33.0
M0	124.6	"	"	20.0 ± 6.8	25.7 8.7	20.0	25.7	26.0	31.7
	125.0	1.0	"	" "	" "	20.0	25.7	21.0	26.7
M4	129.8	"	"	18.2 ± 6.4	23.4 8.2	18.2	23.4	19.2	24.4
M10	134.6	"	"	19.2 ± 6.2	24.6 8.0	19.2	24.6	20.2	25.6
	135.0	"	"	19.1 ± 6.2	24.6 7.9	19.1	24.6	20.1	25.6
	140.0	1.5	"	" "	" "	19.1	24.6	20.6	26.1
M16	142.1	"	"	20.3 ± 6.8	26.1 8.7	20.3	26.1	21.8	27.6
	145.0	1.0	"	20.0 ± 6.9	25.7 8.9	20.0	25.7	21.0	26.7
M21	148.5	"	"	20.9 ± 7.2	26.9 9.3	20.9	26.9	21.9	27.9
	150.0	0.0	"	" "	" "	20.9	26.9	20.9	26.9
M25	154.1	"	"	16.9 ± 5.3	21.8 6.8	16.9	21.8	16.9	21.8
>M25	180.0								

[a] After *Hardebeck and Anderson* [1996].
[b] After *Kaiho and Saito* [1994].
[c] This study, considering either a constant mantle temperature or a 50°C higher temperature of the mantle prior to 80 Ma following *Humler et al.* [1999].
[d] Ocean crust flux of main oceanic basins and back arc basins.
[e] Total crust flux, including plateaus.

accompanied by a suspected ~25 Myr periodicity in the last 75–80 Myr, as we discussed above.

[23] Another point is the role of oceanic plateaus. Oceanic plateaus are a major feature in oceanic crust volume generation [e.g., *Larson*, 1991; *Hardebeck and Anderson*, 1996]. Adding the oceanic volumes proposed by *Hardebeck and Anderson* [1996] to the ridge flux described above, we propose total oceanic crust flux rates without (Table 4; dotted line in Figure 4b) and with (continuous line in Figure 4b) the hypothesis of a larger flux at ridges due to a hotter mantle prior to 80 Ma. Because the oceanic plateaus production appears larger in Cretaceous times, it is obvious that adding them to flux at ridges enhances the higher flux in the Cretaceous, in either hypothesis (Figure 4b). Surprisingly, we notice that our total flux including maximum hypotheses (i.e., plateaus production by *Hardebeck and Anderson* [1996] plus thermal jump at 80 Ma by *Humler et al.* [1999] implying a thicker crust production prior to 80 Ma; Figure 4b) is almost strictly identical in Cretaceous times to the one proposed by *Larson* [1991] but based on the fundamentally different hypothesis of higher spreading rates by that time, associated with a constant thickness of produced crust at ridges, and including some subducted plateaus. At a first level of analysis, and consistent with *Larson* [1991], we thus propose a two-step evolution of oceanic crust flux since 180 Ma, including plateaus and thermal jump of the mantle, with averages at 20.2 ± 3.0 km^3 yr^{-1} in the 0–80 Ma period, and 26.8 ± 3.5 km^3 yr^{-1} in the 80–155 Ma period.

[24] However, a second level of analysis of our results (Table 4, Figure 4b) leads us to propose a second, and double feature. First, it is obvious from Figure 4b that, as we already noticed on production rates (Figure 3b), the general trend of crust flux tends to increase in a significant manner since ~50 Ma. This is in disagreement with all previous works [e.g., *Kominz*, 1984; *Larson*, 1991; *Rowley*, 2002]. If we now turn to older periods, we agree with *Larson* [1991], who suggested a weaker flux rate prior to ~120 Ma. Altogether, this suggests a periodic signal in crust flux with a ~150–200 Myr periodicity. However, we have only one period, and such an assumption must be regarded as tentative.

[25] Second, and more importantly, we provide evidence for a probable ~25 Myr periodicity at least

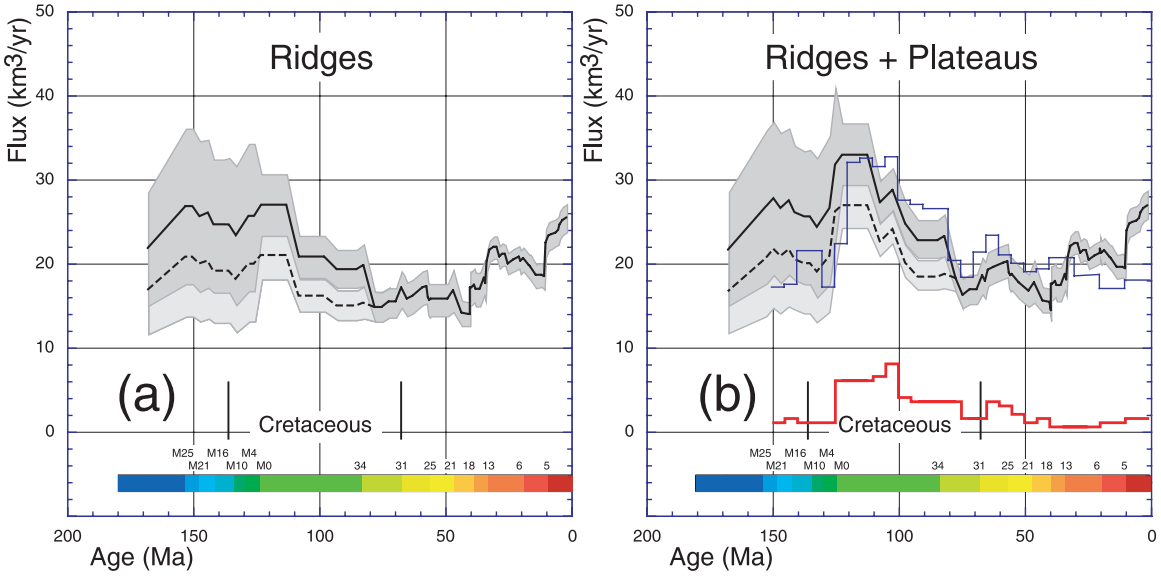

Figure 4. Global oceanic crust flux rates (km^3 yr^{-1}) as a function of time (a) at ridges only and (b) including production of plateaus. Continuous (dotted) black curves: computed with (without) a 50°C thermal jump at 80 Ma in the mantle, as proposed by *Humler et al.* [1999]; gray areas: 2σ confidence areas; blue curve in Figure 4b: following *Larson* [1991]; red curve in Figure 4b: plateau production after *Hardebeck and Anderson* [1996].

in the last 75–80 Myr, obvious in either production or flux rates (Figures 3b and 4). Apart from *Kaiho and Saito* [1994], who proposed a ~35 Myr periodicity mainly based on back arc production rates, it has never been described for oceanic crust production rates at the global scale before.

5. Normalized Fluxes: Discussion

[26] Normalized flux of oceanic crust is an important parameter entering models of global indicators such as sea-level variations [*Vail et al.*, 1977; *Berner*, 1994; *Hardenbol et al.*, 1998] and related global climate proxies such as $\delta^{18}O$ of deep-water foraminifera, atmospheric CO_2 or changes in seawater $^{87}Sr/^{86}Sr$ etc. We provide our evaluations of normalized crust fluxes since 165 Ma (Figure 5, black CH05-max and CH05-min curves), which we compare to 5 previous models. Normalized crust fluxes are expressed as $\{G_{(t)}/G_{(0)}\}$ where $G_{(t)}$ is the flux at time t, and $G_{(0)}$ the present-day flux. Figure 5a shows the change in $\{G_{(t)}/G_{(0)}\}$ of oceanic ridges as a function of time over the last 165 million years. Figure 5b shows how the total oceanic crust production rate (including oceanic plateaus) varies with time.

[27] Indeed, *Kominz* [1984] undertook the first comprehensive study of the oceanic lithosphere production history, after the pioneering work of *Southam and Hay* [1977]. She compiled mean spreading rates (in cm yr^{-1}) and ridge lengths (in km) which we have multiplied to obtain production rates (in km^2 yr^{-1}), over the last 125 Myr. Because of normalization, the $\{G_{(t)}/G_{(0)}\} = f(t)$ curves at ridges may be obtained by the ratio of this production at time t on the production at t_0. From the curves proposed by *Kominz* [1984], we selected the upper (dotted light blue K84-max curve in Figure 5a) and lower (continuous light blue K84-min curve in Figure 5a) hypotheses, which depend on the timescales available at that time. *Engebretson et al.* [1992] used a combination of relative plates motions and reconstructions of subduction zones, in a fixed hot spot reference frame, to assess the time history of subduction, from which they deduce a lithosphere production history which, as normalized, is shown in Figure 5a (green E92 curve). It might be noted that the paleo-Pacific reconstructions of *Engebretson et al.* [1992] partly rely on the hypothesis of a fixity of the Hawaiian hot spots with respect to Atlantic hot spots. More modern analyses [e.g., *Tarduno et al.*, 2003], based on paleomagnetism and ocean drilling, have shown that such might be not the case. Finally, *Rowley* [2002] recently reappraised seafloor production rates (km^2 yr^{-1}) using the ocean age grid of *Royer et al.* [1992] and *Müller et al.* [1997]. Integrating the global differential $\{dA/dt\}$ distribution which, as proposed by *Sclater et al.* [1981] and *Parsons* [1981, 1982], is of the form $\{dA/dt\} = C_0\{1 - t/t_{max}\}$, where C_0 is the present-day production (in km^2 yr^{-1}) and t_{max} the age of the older oceanic crust, the author proposed that the oceanic crust production at ridges remained roughly

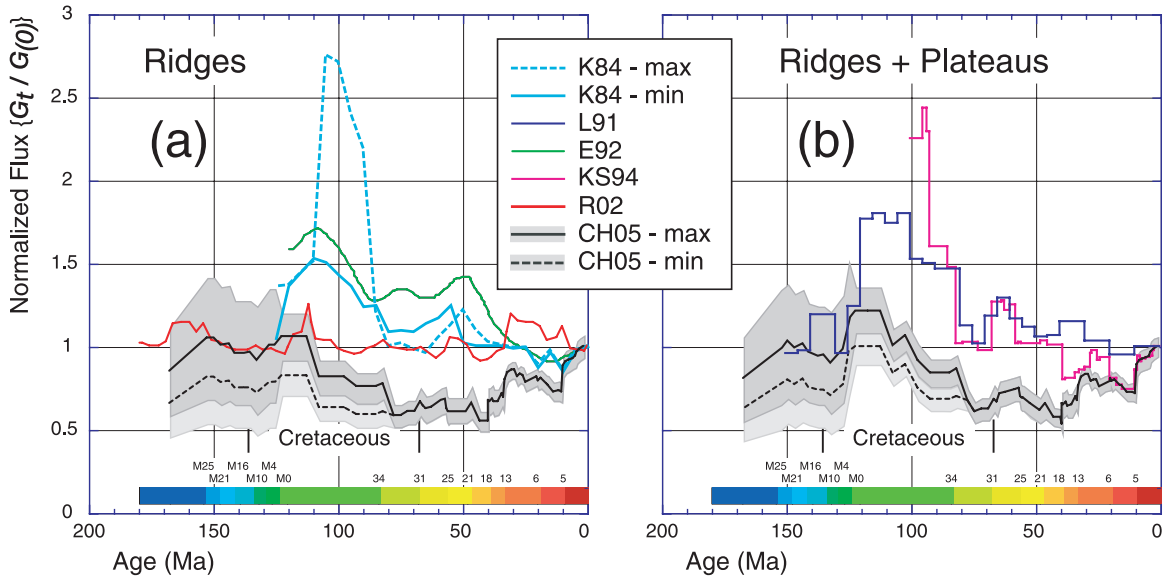

Figure 5. Normalized crust flux $\{G_t/G_{(0)}\}$ (dimensionless) as a function of time (a) at ridges only and (b) including production of plateaus. Black (CH05) curves in Figures 5a and 5b: present study (gray areas, continuous and dotted curves as in Figure 4). (a) Light blue continuous (K84-max) and dotted (K84-min) curves, computed after *Kominz* [1984]; light green curve (E92) after *Engebretson et al.* [1992]; red curve (R02) after *Rowley* [2002]. (b) Blue curve (L91) after *Larson* [1991]; pink curve (KS94) after *Kaiho and Saito* [1994].

constant since 180 Ma at 3.4 km^2 yr^{-1}. The normalized flux curve $\{G_{(t)}/G_{(0)}\} = f(t)$ deduced from *Rowley* [2002] is shown in Figure 5a (red R02 curve). It should be underlined that this curve results from no hypothesis on subducted ridge lengths and passed spreading rates.

[28] Turning to the total flux, including oceanic plateaus production (Figure 5b), we have normalized flux curves of *Larson* [1991] (blue L91 curve) and *Kaiho and Saito* [1994] (pink KS94 curve) to the modern value. The oceanic production of *Larson* [1991] was obtained using spreading rates of *Kominz* [1984] recalibrated using *Harland et al.* [1990] magnetic reversal timescale, and including the plateaus production based on *Schubert and Sandwell* [1989]. *Kaiho and Saito* [1994] made a thorough review of back arc basins surface evolution with time which they transformed to crust flux by multiplying their results by an average 6.5 km crustal thickness at ridges, then adding this to a global flux derived from *Kominz* [1984] and a reappraisal of oceanic plateaus flux.

[29] From Figure 5, it is clear that each of these studies produces a significantly different estimate of past seafloor generation rates. Overall, studies using the most recent isochron database [*Müller et al.*, 1997] give low oceanic lithosphere production rates (R02 and CH05) relative to studies based on older estimations (K84, L91, E92 and KS94). Because of the increase in production during the last 50 Myr which we have documented, our curves (CH05) are significantly lower than previously published results, except for periods older than ~110 Ma (Figure 5a) or ~100 Ma (Figure 5b). In particular, the present study suggests that the present-day production might be ~30% higher than during the ~90–40 Ma period, and on the same order of magnitude than in the beginning of the Cretaceous. Indeed, and consistent with *Rowley* [2002], we do not find a particular ~50 (K84, E92) to 80% (L91) or larger (KS94) pulse of production in the mid-Cretaceous. In contrast, the CH05 curves differ from R02 which, although based on the same isochron data set, does not exhibit any increase in either production or flux rates during the last 50 Myr. This difference is thus clearly linked to the methods used in both studies. Beyond these significant differences between our study and previously published ones, however, some similarities can be found.

[30] First, concerning the increase of crust production in the last few Myr, we note that it is also observed by *Kaiho and Saito* [1994], with a lower amplitude, in the last ~30 Myr (Figure 5b, KS94 curve). Such an increase might also be disclosed in K84 and E92 curves (Figure 5a) in the last 10 to 20 Myr. Second, the ~25 Myr pseudo-periodicity suggested by our results is also obvious in R02 curve (Figure 5a) and KS94 curve (Figure 5b) in the

last 70–80 Myr. It seems to exist also in L91 curve (Figure 5a), but with some time shift with respect to CH05 and KS94 in the 25–40 Ma time interval.

[31] Finally, we have presented only results of computations based on the magnetostratigraphic scale of *Gradstein et al.* [2004a, 2004b]. It should be noted that we made identical computations using the older scale of *Cande and Kent* [1995] and *Gradstein et al.* [1994], as proposed by *Müller et al.* [1997]. These provide results which are in line with the main conclusions we reach here. The increasing oceanic crust flux in the last 50 Myr and the 25 Myr periodicity in the Cenozoic are obvious using both scales. We note that during the Jurassic, where the remaining crust surfaces and ridges are the smaller, the results appear more sensitive to the timescale used. In particular, flux calculations are generally lowered by ~25% based on the older timescale in the 120–150 Ma period relative to the most recent study [*Gradstein et al.*, 2004a, 2004b].

6. Conclusions

[32] We have presented the results of a new evaluation of spreading, production and flux rates of oceanic crust generation. It is based on isochron data proposed by *Royer et al.* [1992] and *Müller et al.* [1997] corrected for the new timescale of *Gradstein et al.* [2004a, 2004b], following the method of *Cogné and Humler* [2004] and using the *PaleoMac* tool of *Cogné* [2003]. From the detailed analysis of 8 oceanic units (North, Central and South Atlantic, West, Central and East Indian, Somalia basin and Pacific) we conclude that while some large variations in spreading rates may occur on a localized scale and at somewhat short periods, the global weighted average rate of spreading on ridges appears constant at 53.4 ± 5.9 (1σ) mm yr^{-1} (full-rate) during the last 125 Myr, consistent with our previous estimates [*Cogné and Humler*, 2004] based on the bulk average of main oceanic plates data. This contradicts the thought that spreading rates were significantly higher in the Cretaceous [*Kominz*, 1984: *Larson*, 1991].

[33] We then computed the global surface production rates $\{dA/dt\}$ as a function of time by adding the modeled production on subducted Tethys and Pacific ridges [*Ricou*, 1994; *Engebretson et al.*, 1985] to the currently observable surfaces production on the globe [e.g., *Sclater et al.*, 1981; *Cogné and Humler*, 2004] for main oceans and to the SOB production proposed by *Kaiho and Saito* [1994]. Consistent with *Rowley* [2002], we see a fairly constant surface production rate of oceanic crust in the last 180 Myr, which we average at 2.7 ± 0.2 km^2 yr^{-1}. At this stage, however, we outline the possibility of a significant 40 to 60% increase of production rate since 50 Ma, accompanied by possible pseudo-periodic fluctuations of ±0.5 km^2 yr^{-1} with a ~25 Myr period, at least during the last 75–80 Myr.

[34] Finally, we propose a new evaluation of oceanic crust production in volume, or flux, at ridges only, and of the total production including plateaus. For both evaluations, we also provide two solutions depending on the existence of thicker crust formation due to higher melt from a hotter mantle as proposed by *Humler et al.* [1999] and *Fisk and Kelley* [2002]. We note that (1) the largest estimate (Table 4, Figure 4b) fits well the proposition of *Larson* [1991] for a larger production in the Cretaceous, although both studies (the present one and the study of *Larson* [1991]) use different approaches; (2) whether we include or not contributions from oceanic plateaus and thermal jump in the mantle [*Humler et al.*, 1999] (Figure 4), we cannot escape the evidence of (i) a general increasing trend in crust production in the last 50 Myr, as we already suggested [*Cogné and Humler*, 2004], which might belong to a ~150–200 Myr periodic phenomenon, and (ii) a ~25 Myr pseudo-periodicity in crust flux, which, apart from *Kaiho and Saito* [1994], but on the scale of back arc basins, has not been reported previously; and (3) the present-day crust flux is on the same order of magnitude than during the early Cretaceous, and about 30% higher than during the middle to late Cretaceous and most of the Cenozoic. We believe that this has a primary significance with respect to other changes of global indicators such as sea-level variations. To treat the effects of changing the seafloor hydrothermal flux, estimates of changes in the seafloor generation rate is needed. For instance, the CO_2 degassing flux from mid-ocean-ridge volcanism has been computed using normalized flux curves reported in Figure 5. If the recent studies of past seafloor generation rate (curves CH05 and R02 in Figure 5) are more accurate than the older estimations, the origin of elevated atmospheric CO_2 levels and global warmth during the Cretaceous linked to mid-ocean ridge magmatism needs to be reconsidered.

Acknowledgments

[35] We dedicate this study to our friend L. E. Ricou, who passed away in December 2005. We thank L. E. Ricou, J. Besse, J. Dyment, Y. Gaudemer, G. Hulot, and F. Fluteau for helpful

discussions and thoughtful insights all along the development of this study. Early drafts of this manuscript were kindly reviewed by J. A. Tarduno, W. Roest, R. D. Müller, M. Tivey, and an anonymous reviewer. This is contribution 2102 of IPGP.

References

Anderson, A. T. (1974), Chlorine, sulfur and water in magmas and oceans, *Geol. Soc. Am. Bull.*, *85*, 1485–1492.

Berner, R. A. (1994), GEOCARB II: A revised model for atmospheric CO_2 over Phanerozoic time, *Am. J. Sci.*, *294*, 56–91.

Berner, R. A., A. C. Lagasa, and R. M. Garrels (1983), The carbonate-silicate geochemical cycle and its effects on atmospheric carbon dioxide over the last 100 million years, *Am. J. Sci.*, *283*, 641–683.

Cande, S. C., and D. V. Kent (1995), Revised calibration of the geomagnetic time scale for the Late Cretaceous and Cenozoic, *J. Geophys. Res.*, *100*, 6093–6098.

Cogné, J. P. (2003), PaleoMac: A Macintosh™ application for treating paleomagnetic data and making plate reconstructions, *Geochem. Geophys. Geosyst.*, *4*(1), 1007, doi:10.1029/2001GC000227.

Cogné, J. P., and E. Humler (2004), Temporal variation of oceanic spreading and crustal production rates during the last 180 My, *Earth Planet. Sci. Lett.*, *227*, 427–739.

Demicco, R. V. (2004), Modelling seafloor-spreading rates through time, *Geology*, *32*, 485–488, doi:10.1130/G20409.1.

Engebretson, D. C., A. Cox, and R. G. Gordon (1985), Relative motions between oceanic and continental plates in the Pacific basin, *Spec. Pap. Geol. Soc. Am.*, *206*, 1–59.

Engebretson, D. C., K. P. Kelly, H. J. Cashman, and M. A. Richards (1992), 180 million years of subduction, *GSA Today*, *2*, 95–100.

Fisk, M., and K. A. Kelley (2002), Probing the Pacific's oldest MORB glass: Mantle chemistry and melting conditions during the birth of the Pacific Plate, *Earth Planet. Sci. Lett.*, *202*, 741–752.

Gradstein, F. M., F. P. Agterberg, J. G. Ogg, J. Hardenbol, P. van Veen, J. Thierry, and Z. Huang (1994), A Mesozoic timescale, *J. Geophys. Res.*, *99*, 24,051–24,074.

Gradstein, F. M., J. G. Oggs, A. G. Smith, W. Bleeker, and L. J. Lourens (2004a), A new geologic time scale with special reference to Precambrian and Neogene, *Episodes*, *27*, 83–100.

Gradstein, F. M., et al. (2004b), *A Geologic Time Scale 2004*, 589 pp., Cambridge Univ. Press, New York.

Hardebeck, J., and D. L. Anderson (1996), Eustasy as a test of a Cretaceous superplume hypothesis, *Earth Planet. Sci. Lett.*, *137*, 101–108.

Hardenbol, J., J. Thierry, M. B. Farley, P. C. de Graciansky, and P. R. Vail (1998), Mesozoic and Cenozoic sequence chronostratigraphic framework of European basins, in *Mesozoic and Cenozoic Sequence Stratigraphy of European Basins*, edited by P. C. de Graciansky et al., *Spec. Publ. SEPM Soc. Sediment. Geol.*, *60*, 3–13.

Harland, W. B., R. L. Armstrong, A. V. Cox, L. E. Craig, A. G. Smith, and D. G. Smith (1990), *A Geologic Time Scale*, 263 pp., Cambridge Univ. Press, New York.

Hays, J. D., and W. C. Pitman, III (1973), Lithospheric plate motion, sea level changes and climatic and ecological consequences, *Nature*, *246*, 18–22.

Humler, E., and J. Besse (2002), A correlation between mid-ocean-ridge basalt chemistry and distance to continents, *Nature*, *419*, 607–609.

Humler, E., J. L. Thirot, and J. P. Montagner (1993), Global correlations of ocean ridge basalt chemistry with seismic tomographic images, *Nature*, *364*, 225–228.

Humler, E., C. H. Langmuir, and V. Daux (1999), Depth versus age: New perspectives from the chemical compositions of ancient crust, *Earth Planet Sci. Lett.*, *173*, 7–23.

Kaiho, K., and S. Saito (1994), Oceanic crust production and climate during the last 100 Myr, *Terra Nova*, *6*, 376–384.

Klein, E. M., and C. H. Langmuir (1987), Global correlations of ocean ridge basalt chemistry with axial depth and crustal thickness, *J. Geophys. Res.*, *92*, 8089–8115.

Kominz, M. (1984), Oceanic ridge volumes and sea-level change—An error analysis, *AAPG Mem.*, *36*, 109–127.

Langmuir, C. H., E. M. Klein, and T. Plank (1992), Petrological systematics of mid-ocean ridge basalts: Constraints on melt generation beneath oceanic ridges, in *Mantle Flow and Melt Generation at Mid-Ocean Ridges*, *Geophys. Monogr. Ser.*, edited by J. Phipps Morgan et al., vol. 71, pp. 183–280, AGU, Washington, D. C.

Larson, R. L. (1991), Latest pulse of the Earth: Evidence for a mid-Cretaceous superplume, *Geology*, *19*, 547–550.

Machetel, P., and E. Humler (2003), High mantle temperature during Cretaceous avalanche, *Earth Planet. Sci. Lett.*, *208*, 125–133.

McKenzie, D. (1984), The generation and compaction of partially molten rock, *J. Petrol.*, *25*, 713–765.

Müller, R. D., W. R. Roest, J. Y. Royer, L. M. Gahagan, and J. G. Sclater (1997), Digital isochrons of the world's ocean floor, *J. Geophys. Res.*, *102*, 3211–3214.

Parsons, B. (1981), The rates of plate consumption and creation, *Geophys. J. R. Astron. Soc.*, *67*, 437–448.

Parsons, B. (1982), Causes and consequences of the relation between area and age of the ocean floor, *J. Geophys. Res.*, *87*, 289–303.

Patriat, P., and J. Achache (1984), India-Eurasia collision chronology has implications for crustal shortening and driving mechanism of plates, *Nature*, *311*, 615–621.

Ricou, L. E. (1994), Tethys reconstructed: Plates, continental fragments and their boundaries since 260Ma from Central America to South-eastern Asia, *Geodin. Acta*, *7*(4), 169–218.

Rowley, D. B. (2002), Rate of plate creation and destruction: 180Ma to present, *Geol. Soc. Am. Bull.*, *114*, 927–933.

Royer, J. Y., R. D. Müller, L. M. Gahagan, L. A. Lawyer, C. L. Mayes, D. Nürnberg, and J. G. Sclater (1992), A global isochron chart, *Tech. Rep. 117*, Inst. for Geophys., Univ. of Tex., Austin.

Schilling, J. G., C. K. Unni, and A. E. Bender (1978), Origin of chlorine and bromine in the oceans, *Nature*, *273*, 631–636.

Schubert, G., and D. Sandwell (1989), Crustal volumes of the continents and of oceanic plateaus and continental submarine plateaus, *Earth Planet. Sci. Lett.*, *92*, 234–246.

Sclater, J. G., B. Parsons, and C. Jaupart (1981), Oceans and continents: Similarities and differences in the mechanisms of heat loss, *J. Geophys. Res.*, *86*, 11,535–11,552.

Southam, J. R., and W. W. Hay (1977), Time scales and dynamic models of deep-sea sedimentation, *J. Geophys. Res.*, *82*, 3825–3842.

Tarduno, J. A., et al. (2003), The Emperor Seamounts: Southward motion of the Hawaiian hotspot plume in Earth's mantle, *Science*, *301*, 1064–1069.

Vail, P. R., R. M. Mitchum, Jr., and S. Thompson, III (1977), Seismic stratigraphy and global changes of sea level, Part 4: Global cycles of relative changes of sea level, *Mem. Am. Assoc. Pet. Geol.*, *26*, 83–97.

Wilson, M. (1989), *Igneous Petrogenesis: A Global Tectonic Approach*, 466 pp., CRC Press, Boca Raton, Fla.